New insights into formation of Ni-based alloyed Ohmic contacts to GaAs

G. Rajaram, T. S. Abhilash and Ch. Ravi Kumar

School of Physics and Centre for Nanotechnology, University of Hyderabad, Prof. C. R. Rao Road,
Gachibowli, Hyderabad 500 046, Andhra Pradesh, India.
e-mail:grrsp@uohyd.ernet.in, Ph: +91-40-2313 4319

Keywords: GaAs/AlGaAs, 2DEG, Hall Sensors, HEMT, Alloyed Ohmic Contacts, Magnetism of Ni

Abstract

Magnetic properties of AuGe/Ni/Au Ohmic contact for use in fabrication of high sensitivity Hall magnetic field sensors with integrated FET circuits, utilizing GaAs/AlGaAs 2DEG, are investigated. Measurements indicate that Ni undergoes solid-state, solubility limited dissolution into the AuGe layer during the anneal, and prior to alloying of the metallization structure for the formation of Ohmic contact. This results in increase of the melting temperature of the AuGe layer. The ohmic contact structure is rendered non-magnetic upon annealing and prior to the alloying. Therefore, the conventional process Ohmic contact process can be used for integrating Hall sensors with FET and pHEMT in monolithic form.

INTRODUCTION

GaAs/AlGaAs multilayer structures, incorporating the 2DEG layer have well known applications in infrared sources/detectors and in high-speed electronic devices e.g. HEMT [1-3]. The 2DEG structures also have another, a not-so-familiar application in fabrication of high sensitivity Hall effect magnetic field sensors for magnetic phase-diagram determination and magnetic microscopy studies [4-6]. Researchers in this area have tended to use variations of the well tested recipe (AuGe/Ni/Au) [7-11], by replacing Ni with non-ferromagnetic materials such as Cr or Ti for Ohmic contact formation. This variation was motivated by the possible distortion of the measured field by the ferromagnetic Ni. However, this involves a trade-off in contact resistance and surface morphology. This trade-off is particularly disadvantageous if HEMT circuits are to be integrated with the sensor on the same substrate.

Our Studies provide new insight into changes of magnetic properties of Ohmic contact to GaAs during Ohmic contact formation process. This subject has received little attention in the literature.

EXPERIMENTAL DETAILS

The GaAs/AlGaAs multilayer structure (table I) used in this study was grown by Molecular Beam Epitaxy (MBE). Metallizations with three AuGe compositions - eutectic (88:12 wt %) and off-eutectics (95:5 and 97.3:2.7 wt %) – were examined (table 1). AuGe and Au layers were deposited by thermal evaporation and Ni layer by electron beam evaporation. The contact resistance was measured by lithographically patterning a transmission line pattern as described in [12] and using the Transfer Length Model (TLM) [13].

TABLE I
EPI AND OHMIC CONTACT STRUCTURES

Au (200nm)	
Ni (10-100nm)	
AuGe (100nm)	
n^+ (Si 1.5 x 10^{18}) GaAs	20nm Cap layer
n^+ (Si 1.5 x 10^{18}) $Al_{0.3}GaAs_{0.7}$	30nm Supply layer
Intrinsic AlGaAs	15nm Separation layer
Intrinsic GaAs	500nm **2DEG**
SI GaAs Substrate	500μm

Magnetic measurements were carried out using a Vibrating Sample Magnetometer on 4 mm^2 samples that were rapid thermal annealed and cooled down to room temperature. Atomic force microscopy (AFM) and conducting probe AFM was used to study the morphology and to map the current distribution through the alloyed contact surface. Grazing incidence XRD and SEM were used to study the changes in the metallization structure on annealing.

RESULTS AND DISCUSSION

The contact resistance and surface roughness, as a function of Ni layer thickness with three AuGe compositions are summarized in table II.

TABLE II
CONTACT RESISTANCE WITH DIFFERENT Ni LAYER THICKNESSES

AuGe alloy composition (wt %)	*Nickel layer thickness (nm)*	*Contact resistance (Ω-mm)*	*RMS Surface roughness (nm)*
88:12	25	0.05±0.01	21 ± 3
88:12	30	0.07 ±0.005	20± 2
88:12	50	0.90	11± 1
95:5	30	0.17 ±0.02	5.5 ±0.5
97.3:2.7	30	1.30	4.5 ±0.5

The minimum in the contact resistance is obtained for Ni layer thickness of 25-30 nm. Increasing the Ni layer thickness or decreasing the Ge content from the eutectic AuGe alloy decreases the surface roughness but increases the contact resistance. The use of off-eutectic composition of the AuGe alloy (95:5) is a better compromise for trading off contact resistance for smoother surface than increasing Ni layer thickness (table II). The contact resistance and roughness depend on the Ni/AuGe thickness *ratio* rather than on absolute values.

The room temperature magnetic hysteresis loops of AuGe (100nm)/Ni (50nm)/Au (200nm) upon annealing is shown in Figure 1. The as-deposited film structures are ferromagnetic. The magnetization progressively decreases to zero as the anneal temperature is increased (Fig. 1 and table III). The decrease in magnetization at anneal temperature as low as 100°C, indicates that the change has begun in the as-deposited film. The results confirm that contacts prepared by the conventional recipe are non-magnetic.

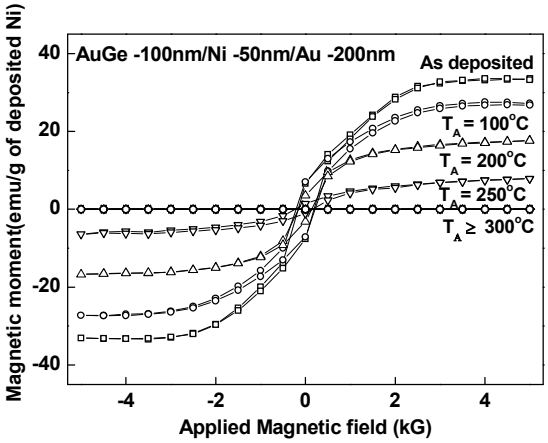

Figure 1. Magnetization loops for AuGe/Ni(50 nm)/Au annealed at various anneal temperatures.

Figure 2 shows the magnetization data for metallizations with same Ni/AuGe ratio. The data show that the amount of Ni converted to non-magnetic phase is proportional to the AuGe layer thickness (table III).

TABLE III
MAGNETIZATION DATA FOR DIFFERENT Ni LAYER THICKNESSES

AuGe alloy composition (wt %)	*AuGe layer thickness (nm)*	*Nickel layer thickness (nm)*	*Anneal Temperature at which Ni is transformed to non-magnetic compounds (°C)*
88:12	100	25	200-250
88:12	100	30	200-250
88:12	100	50	250-300
88:12	100	75	350-400
88:12	50	25	250-300
88:12	150	75	250-300
95: 5	100	30	250-300
97.3:2.7	100	30	400-430

This dependence implies that entire AuGe layer, and not just the interface, participates in the conversion of Ni layer to a non-magnetic phase i.e. Ni dissolves into AuGe.

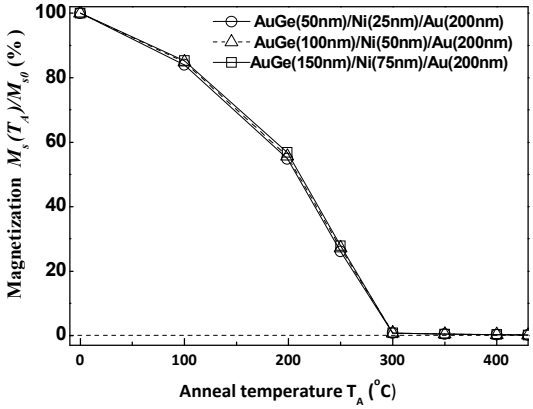

Figure 2. Anneal temperature dependence of saturation magnetization of contacts with same Ni/AuGe ratio.

Magnetization measurements as function of anneal durations (before alloying), show that the transformed Ni fraction is independent of time (for time scales ~15 minutes) (Fig. 3) and depends only on anneal temperature. Thus Ni dissolution into AuGe appears to be solubility limited rather than diffusion limited at these time and temperature scales.

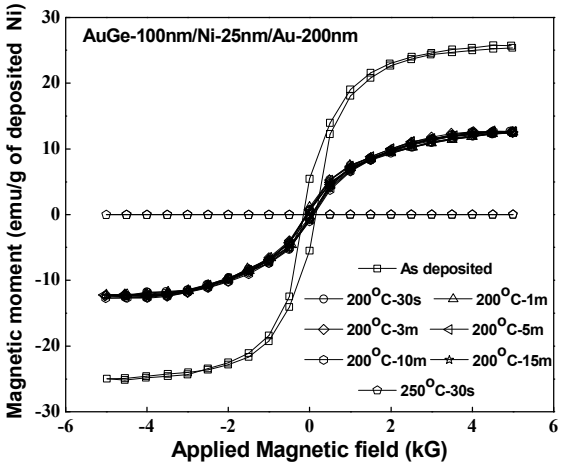

Figure 3. Magnetization as a function of anneal durations.

Figure 4 demonstrates that a quantity proportional to the Ni-layer thickness transformed to the non-magnetic phase increases with anneal temperature and is independent of initial Ni layer thickness until all the Ni is transformed. The solubility of Ni in AuGe increases with anneal temperature and decreases with decreasing Ge content in the AuGe alloy. Cross sectional SEM micrographs show two distinct layers in a sample where the magnetic to non magnetic transformation is complete but no alloying has yet taken

place. The dissolution of Ni into AuGe appears to occur in the solid state phase.

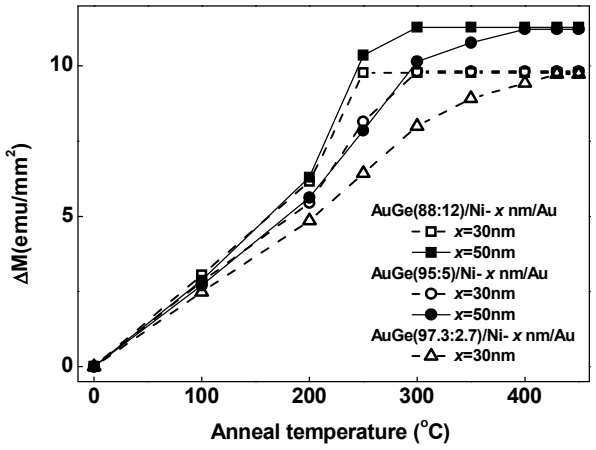

Figure 4. Effective thickness of Ni layer transformed to non-magnetic phase on annealing at various temperatures.

GIXRD data on a sample (AuGe (88:12)/Ni-25nm/Au) annealed at 300°C, and cooled down to room temperature indicates the formation of NiGe, when the structure is rendered non-magnetic. A picture consistent with these results is that *Ni dissolves into AuGe in a solid-state solubility-limited process* and precipitates into non-magnetic NiGe compounds on cooling.

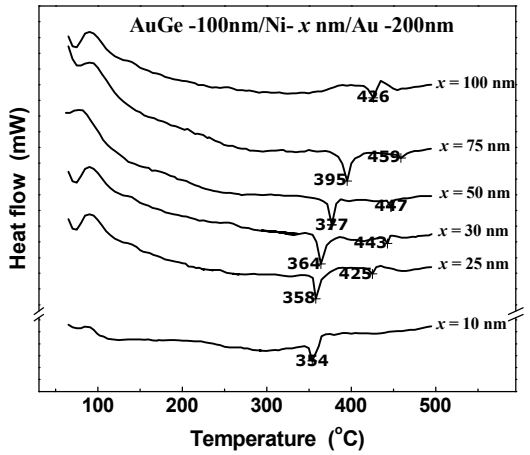

Figure 5. DSC scans for samples with eutectic AuGe alloy and different Ni layer thicknesses.

Alloying between the metallization structure and the substrate seems to occur at higher temperatures ~400°C. DSC scans indicate that the Ni dissolution into AuGe influences melting and alloying characteristics of the metallization structure. The melting temperature of the metallization structure increases with increasing initial Ni layer thickness and decreasing Ge content from that of the eutectic AuGe alloy, consistent with in-situ XRD studies [14]. The evidence that these DSC peaks are signatures of melting come from the surface roughness data as functions of anneal temperature, for eutectic AuGe alloys with different Ni layer thicknesses.

Adhesion studies by scratch test (Fig.6) conclude that the film's scratch resistance or adhesion improves as the anneal temperature is increased (prior to alloying) as well as with increasing Ni layer thickness (i.e. with increasing dissolved Ni in AuGe).

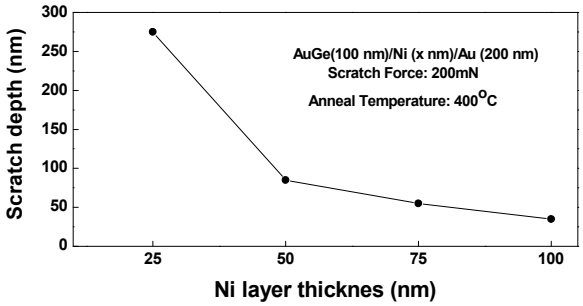

Figure 6. Scratch depth *Vs.* Ni layer thickness.

Solid state diffusion creates a saturated solution of Ni in AuGe at temperatures below that at which final alloying the Ohmic contacts with the substrate, occurs. The DSC and roughness data indicate that the effect of this dissolution is to increase the melting temperature of the structure. This could be the possible reason for improvement of surface roughness with increasing Ni layer thickness. However, use of excessive Ni layer deteriorates contact resistance.

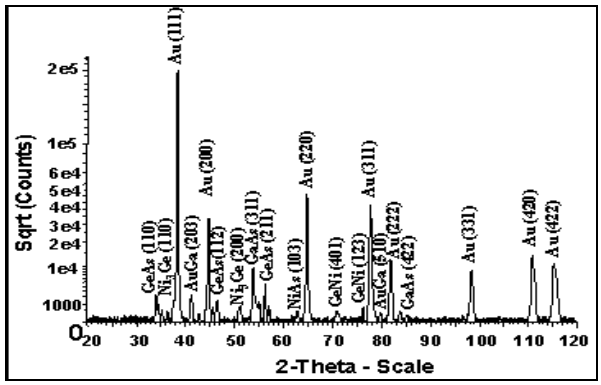

Figure 7. GIXRD measurements on AuGe/Ni (25nm)/Au annealed at 400°C and which shows the least contact resistance.

Possible reasons for this deterioration are indicated by the GIXRD results on samples annealed at temperature at which alloying take place (Fig.7). Formation of phases such as NiGe and NiAs, AuGa is observed, on cooling. Other data in the literature indicate the presence of Ni_3Ge phase for samples cooled down from higher temperature anneals and with larger Ni thickness, finally forming Ni_2GeAs and AuGa phases when alloying takes place [15-18].

The increase in contact resistance could possibly be due to the reduced availability of Ge for doping into GaAs and carrier compensation due to out-diffusion of As. The current distribution of annealed AuGe/Ni (30nm)/Au (Fig. 8)

contacts shows, unexpectedly, short range spatial in-homogeneities, implying that 1) the integrity of the Au overlayer is severely affected during the melting/alloying process and 2) possible presence of precipitates at the substrate-metallization interface, eg. the molten AuGa phases resulting from alloying and from the Ni-Ge or Ni-Ge-As precipitates respectively.

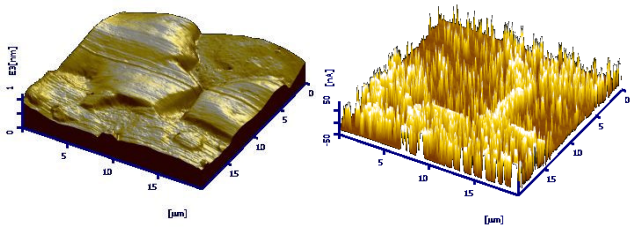

Figure 8. (a) Topography and (b) current image of an AuGe/Ni (30nm)/Au sample.

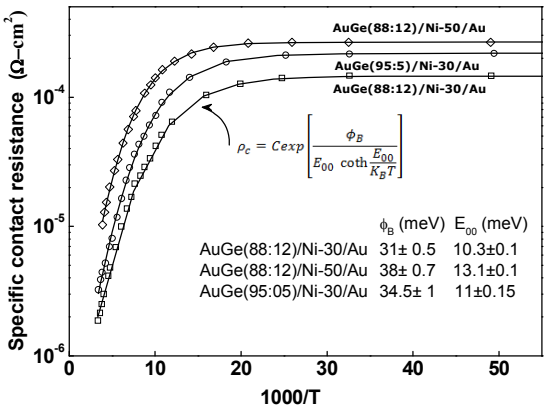

Figure 9. Specific contact resistance plotted as a function of inverse temperature for three AuGe alloy with different Ni layer thickness.

Low temperature dependence of contact resistance performed down to 4K (Fig. 9) displays both tunnelling and thermionic emission characteristics [19-20]. The effective barrier height as well as tunnelling transmission coefficient, obtained by fitting the data to a 'thermal field emission' model, show an increase with enhanced Ni layer thickness or decreased Ge content in the AuGe alloy in relation to the optimal structure (eutectic AuGe with 30nm Ni). A parallel conduction via the two mechanisms through physically distinct areas, is also very likely and needs to be examined.

CONCLUSIONS

The metallization structures are rendered non-magnetic at room temperature after annealing at typically used alloying conditions. The magnetic measurements are suggestive of solid-state solubility-limited dissolution of Ni into AuGe followed by segregation into non magnetic Ni-Ge compounds on cooling. Increase of initial Ni-layer thickness and decrease of Ge content results in higher melting temperature and less surface roughness. The optimum (lowest) contact resistance (0.05±0.01 Ω-mm) is obtained at a Ni layer thickness of 25-30nm. The surface roughness decreases on decreasing Ge content in the alloy or increasing the Ni layer thickness. Decreasing Ge content, however, seems a better choice for trading off contact resistance for surface smoothness. The current distribution on the surface is non-uniform with short and long range fluctuations.

ACKNOWLEDGMENTS

Support of UGC (UPE, CAS programmes), BRNS/DAE, IGCAR, DST (Centre for Nanotechnology) is acknowledged.

REFERENCES

[1] A. Kock, E. Gornik, G. Abstreiter, G. Bohm, M. Walther, G. Weimann, Applied Physics Letters **60**, no.16, 2011 (1992).
[2] T. R. Lepkowski, G. Shade, S. P. Kwok, M. Feng, L. E. Dickens, D. L. Laude, B. Schoendube, IEEE Electron Device Letters **7**, no. 4, 222 (2005).
[3] H. Lafontaine, A. M. Haghiri-Gosnet, Y. Jin, P. Crozat, R. Adde, M. Chaker, H. Pepin, F. Rousseaux, H. Lounois, IEEE Trans. Electron Devices., **43**, no. 1, 175 (1996).
[4] Yoshinobu Sugiyama, J. Vac. Sci. Technol. B. **13**, no. 3, 1075 (1995).
[5] Y. Yamaguchi, G. Rajaram, N. Shirakawa, A. Mumtaz , H. Obara, T. Nakagawa and H. Bando, Physical Review B. **63**, no.1, 14504 (2000).
[6] Adarsh Sandhu, Hiroshi Masuda, Ahmet Oral and Simon J. Bending, Jpn. J. Appl. Phys. **40**, 4321 (2001).
[7] R. P. Taylor, P. T. Coleridge, M. Davies, Y. Feng, J. P. McCaffrey and P. A. Marshall, J. Appt. Phys. **76**, no. 12, 7966 (1994).
[8] A. Ketterson, F. Ponse, T. Henderson, J. Klem and H. Morkoç, J. Appl. Phys. **57**, no. 6, 2305 (1985).
[9] Soo-Jin Chua and Seng Hin Lee, Jpn. J. Appl. Phys. **33**, 66 (1994).
[10] N. Braslau, J. B. Gunn and J. L. Staples, Solid State Electron. **10**, 381 (1967).
[11] O. Goktas, J. Weber, J. Weis and Klaus von Klitzing, Physica E. **40**, 1579 (2007).
[12] T S Abhilash, Ch Ravi Kumar and G Rajaram, J. Phys. D: Appl.Phys. **42**, 125104 (2009).
[13] H. H. Berger, Solid State Electron. **15**, no. 2, 145 (1972).
[14] Taeil Kim and D.D.L. Chung, Thin Solid films **147**, no. 2, 177 (1986).
[15] Masanori Murakami, Science and Technology of Advanced Materials **3**, 1 (2002).
[16] M. Ogawa, J. Appl. Phys. **51**, no. 1, 406 (1980).
[17] T. S. Kuan, P. E. Batson, T. N. Jackson, H. Rupprecht and E. L. Wilkie, J. Appl. Phys. **54**, no. 12, 6952 (1983).
[18] G. Sai Saravanan, K. Mahadeva Bhat, K. Muraleedharan, H. P. Vyas, R. Muralidharan and A. P. Pathak, Semicond. Sci. Technol. **23**, 025019 (2008).
[19] T. S. Abhilash, Ch. Ravi Kumar, B. Sreedhar, G. Rajaram, Semicond. Sci. Technol. **25**, 035002 (2010).
[20] T. C. Shen, G. B. Gao and H. Morkoc, J. Vac. Sci. Technol. B. **10**, 2113 (1992).

ACRONYMS

2DEG: Two Dimensional Electron Gas
HEMT: High Electron Mobility Transistor
SEM: Scanning Electron Microscope
DSC: Differential Scanning Calorimetry
GIXRD: Grazing Incidence X-Ray Diffraction